Received: 6 May 2020 | Revised: 24 July 2020 | Accepted: 27 July 2020

DOI: 10.1002/mrm.28479

FULL PAPER

Magnetic Resonance in Medicine

A novel sequence to improve auditory functional MRI with variable silent delays

Manoj Shrestha[1] | **H. Sean Lee**[2] | **Ulrike Nöth**[1] | **Ralf Deichmann**[1]

[1]Brain Imaging Center (BIC), Goethe University Frankfurt, Frankfurt am Main, Germany

[2]Max Planck Institute for Empirical Aesthetics, Frankfurt am Main, Germany

Correspondence
Manoj Shrestha, Brain Imaging Center (BIC), Goethe University Frankfurt, Schleusenweg 2-16, 60528 Frankfurt am Main, Germany.
Email: shrestha@med.uni-frankfurt.de

Purpose: Auditory functional MRI (fMRI) often uses silent inter-volume delays for stimulus presentation. However, maintaining the steady-state of the magnetization usually requires constant delays. Here, a novel acquisition scheme dubbed "pre-Saturated EPI using Multiple delays in Steady-state" (SEPIMS) is proposed, using spin saturation at a fixed delay before each volume to maintain steady-state conditions, independent of previous spin history. This concept allows for variable inter-volume delays and thus for flexible stimulus design in auditory fMRI. The purpose was to compare the signal stability of SEPIMS and conventional sparse EPI (CS-EPI).

Methods: The saturation module comprises two non-selective adiabatic saturation pulses. The efficiency of the saturation and its effect on the SEPIMS signal stability is tested in vitro and in vivo.

Results: Data show that SEPIMS yields the same signal stability as CS-EPI, even for extreme variations between inter-volume delay durations. However, dual saturation pulses are required to achieve sufficiently high saturation efficiency in compartments with long T_1 values. Importantly, spoiler gradient pulses after the EPI readout have to be optimized to avoid eddy-current-induced image distortions.

Conclusion: The proposed SEPIMS sequence maintains high signal stability in the presence of variable inter-volume durations, thus allowing for flexible stimulus design.

KEYWORDS

adiabatic saturation, auditory fMRI, scanner noise, sparse imaging, steady-state condition, variable silent delay

1 | INTRODUCTION

Functional MRI (fMRI) of the auditory system is challenging due to interference of gradient noise with the presented auditory stimuli. This may cause additional activation of the auditory cortex, interacting with the stimulus-induced activation patterns of interest. In extreme cases, scanner noise can completely mask the acoustic stimuli. To avoid this problem, special pulse sequences are required.

Echo-planar imaging (EPI)[1] is the most commonly used sequence in fMRI studies. However, EPI requires rapid switching of a strong readout gradient, generating marked acoustic

noise which may hamper investigations of the auditory cortex via fMRI. To avoid acoustic interference in cognitive and systems neuroscience studies investigating the perception of language and music, sparse sampling[2-4] is frequently used, interleaving EPI acquisitions with silent periods for presenting sound stimuli. Such conventional sparse EPI (CS-EPI) maintains a constant steady state of the longitudinal magnetization by keeping silent inter-volume delays constant throughout the measurement. However, the CS-EPI method has some disadvantages. As an example, it has been described that the method requires prior assumptions about the time-to-peak of the hemodynamic blood oxygen level-dependent (BOLD) response, and that the sparse acquisition of single volumes after each silent delay reduces the amount of data available, thus leading to poor statistical power.[5] In general, the choice of a constant time interval for acoustic stimulus presentation is not an ideal solution for certain experimental designs. For example, sampling of the hemodynamic response curve may be facilitated using variable delays during the measurement. To address these problems, the interleaved silent steady state (ISSS) sampling scheme[5] was proposed where steady-state conditions of the longitudinal magnetization are maintained during the inter-volume delays via a train of slice selective radiofrequency (RF) pulses without subsequent data acquisition. However, the required slice selective gradient pulses still cause a certain level of scanner noise, requiring careful design of the gradient wave forms.[5]

In this study, a novel acquisition scheme dubbed "pre-Saturated EPI using Multiple delays in Steady-state" (SEPIMS) is presented, allowing for the insertion of silent inter-volume delays with variable duration. Steady-state conditions are maintained via robust spin saturation at fixed time points before each EPI acquisition. This steady state is independent of the spin history prior to the saturation, allowing for the insertion of silent delays of arbitrary length at this position. Thus, SEPIMS overcomes the constraint of a constant inter-volume delay as in CS-EPI and allows for multiple options in audio stimulus design. However, it should be noted that any residual bias of the inter-volume delay on the SEPIMS signal intensity will yield false activation upon functional analysis of the data. This poses high demands on the SEPIMS signal stability. In particular, the following conditions have to be met: (1) the saturation efficiency in SEPIMS must be high, so the signal intensity is independent of the previous spin history. (2) Spoiler gradient pulses following the EPI readout have to be optimized to reduce eddy currents that may induce distortions in subsequent images, in dependence on inter-volume delay durations. In a recent publication, it was shown that eddy currents may in fact have slowly decaying components, requiring dummy scans with a duration of up to 1.5 s for achieving a steady state.[6] Thus, in the case of variable inter-volume delays, data acquired after a short delay may be more affected by eddy currents, again yielding a bias that may result in false positives/negatives upon functional analysis. In the present study, the signal stabilities of SEPIMS and CS-EPI are compared in vitro and in vivo, using a short and a long inter-volume delay in an alternating fashion. Data are analyzed in two ways: (1) a region of interest (ROI) based analysis of the time course of signal intensities, the ROI comprising either the whole phantom or separately white matter (WM), gray matter (GM), and cerebrospinal fluid (CSF) in the in vivo experiments. (2) A functional analysis, testing for systematic differences between signal intensities of even and odd volumes.

2 | METHODS

2.1 | Pulse sequences

Figure 1 shows schematically three different pulse sequences used in this study for auditory fMRI. Figure 1A shows the conventional CS-EPI sequence, using a constant inter-volume delay τ for presenting auditory stimuli while maintaining the steady-state. It should be noted that the use of variable τ values would yield a different longitudinal magnetization before each EPI acquisition, thus inducing signal variations that would mask stimulus-related effects. Figure 1B shows the SEPIMS sequence with spin saturation at a constant delay τ_{sat} prior to the EPI readout, induced via a single saturation pulse (SSP) per delay. Here, it is possible to use different delays (τ_1 and τ_2) between volumes as the introduction of an additional delay before the saturation does not affect the magnetization, provided τ_{sat} remains constant and complete spin saturation is achieved. As for standard sparse sampling, in SEPIMS, a single EPI volume is acquired after each inter-volume delay. To improve spin saturation, a second version of the proposed SEPIMS sequence with dual saturation pulses (DSP) was designed, as presented in Figure 1C. In the current implementation, two alternating silent periods τ_1 and τ_2 in the pre-saturation module were used between successive EPI volumes.

For optimum spin saturation that is immune to typical non-uniformities of the transmitted RF magnetic field (B_1), a non-selective adiabatic pulse dubbed "B_1 independent rotation" (BIR) was used, in particular the four-segment version (BIR-4) as described by Staewen et al.[7]

The pulse was designed according to the literature,[7] using the following parameters: number of sample points $N = 2000$, duration of 8000 μs, constant values $\beta = 10$, $\kappa = \tan^{-1}(10)$ for the adiabacity of the pulse, and $\varphi_0 = 100 \cdot \pi$ for the phase calculation. Furthermore, for a nominal saturation angle of $\alpha = \pi/2$, the complex pulse profile requires a phase offset $\Delta\varphi = \pi + \alpha/2$ for the second and third segment (see below).

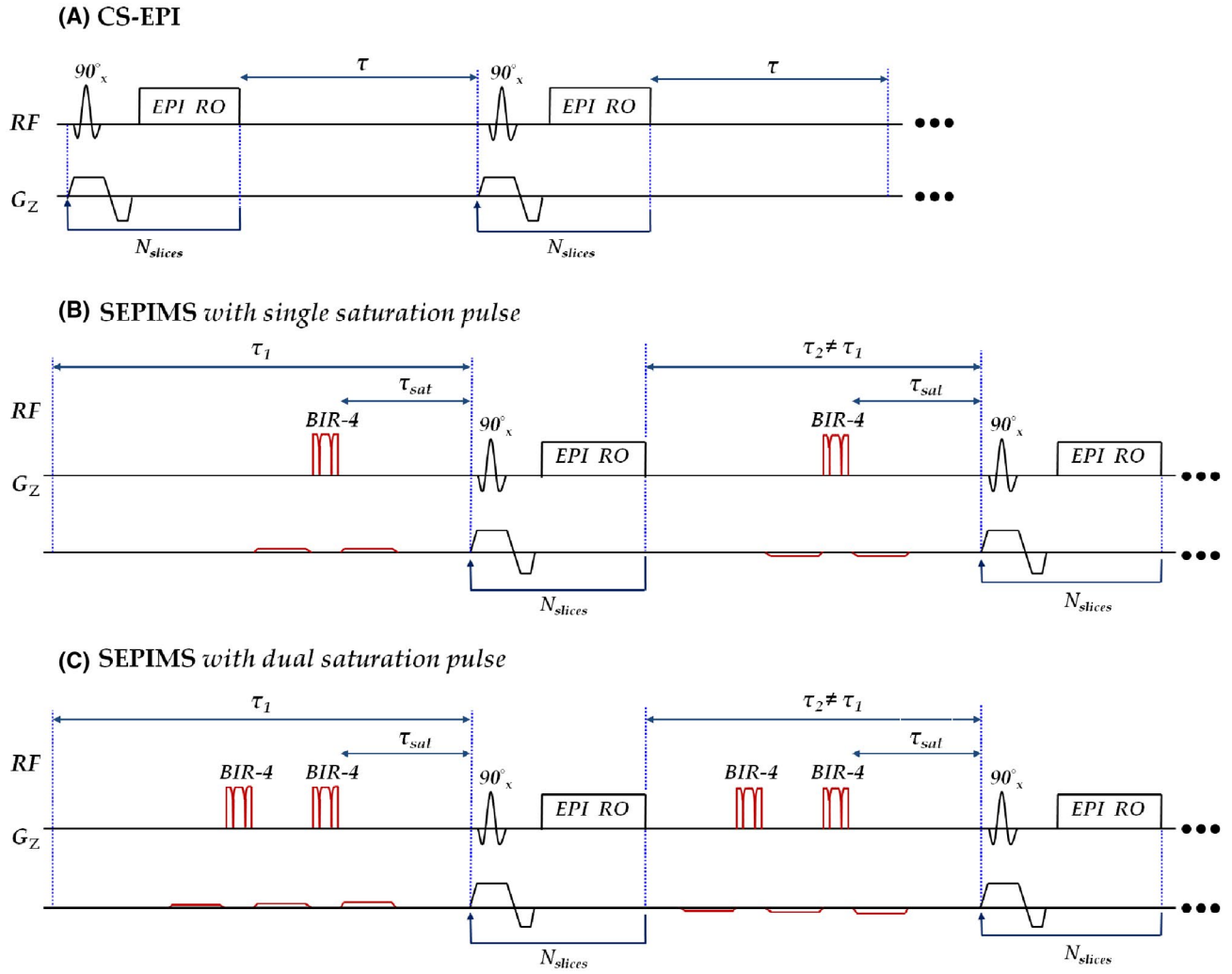

FIGURE 1 Schematic representation of the different pulse sequences for auditory fMRI. A, Conventional sparse EPI (CS-EPI) with a fixed inter-volume delay τ. B, SEPIMS with single saturation pulse and two different inter-volume delays τ_1 and τ_2 between EPI volumes. Signal steady-state conditions are achieved via spin saturation at a constant delay τ_{sat} prior to every EPI volume acquisition. For saturation, single adiabatic BIR-4 pulses between very weak spoiling gradients are used. C, The proposed SEPIMS with dual saturation pulse for improved saturation efficiency

The four segments were designed by defining for each sample point i ($0 \le i < N$) the amplitude $A(i)$ and the phase $\varphi(i)$. Furthermore, the variable λ was introduced according to $\lambda_i = (0.5 + i) \cdot 4/N$, ranging from 0 to 4 across the four segments. The amplitude factor A_0 was chosen as described later in this section.

Segment 1 for $0 \le i < N/4$ and $0 < \lambda < 1$:

$$A_1(i) = A_0 \tanh\left[\beta\left(1-\lambda_i\right)\right]$$

$$\varphi_1(i) = \frac{\varphi_0}{4\kappa \cdot \tan(\kappa)}\left\{-\ln\left[\cos\left(\kappa \cdot \lambda_i\right)\right]\right\}. \quad (1)$$

Segment 2 for $N/4 \le i < N/2$:

$$A_2(i) = A_1\left(\frac{N}{2}-1-i\right)$$

$$\varphi_2(i) = \varphi_1\left(\frac{N}{2}-1-i\right). \quad (2)$$

Introducing the index variable $i' = i - N/4$, which starts from 0 at the beginning of segment 2, this can be written as:

$$A_2\left(i'\right) = A_1\left(\frac{N}{4}-1-i'\right)$$

$$\varphi_2\left(i'\right) = \varphi_1\left(\frac{N}{4}-1-i'\right). \quad (3)$$

Thus, segment 2 corresponds to segment 1, being mirrored around sample point $N/4$.

Segments 3 and 4 for $N/2 \le i < N$:

$$A_{3/4}(i) = A_{1/2}(N-1-i)$$

$$\varphi_{3/4}(i) = \varphi_{1/2}(N-1-i). \quad (4)$$

Introducing the index variable $i'' = i - N/2$, which starts from 0 at the beginning of segment 3, this can be written as:

$$A_{3/4}(i'') = A_{1/2}\left(\frac{N}{2}-1-i''\right)$$

$$\varphi_{3/4}(i'') = \varphi_{1/2}\left(\frac{N}{2}-1-i''\right). \quad (5)$$

Thus, the combination of segments 3 and 4 corresponds to the combination of segments 1 and 2, being mirrored around sample point $N/2$. Finally, for segments 2 and 3, the phase values $\varphi(i)$ were increased by $\Delta\varphi$ as defined above to achieve the correct saturation angle.

The lists of amplitude and phase values were calculated for each segment of the BIR-4 pulse. The amplitude factor A_0 was chosen in a way that the maximum amplitude of the BIR-4 pulse was 17.78 times larger than the amplitude of a rectangular 90° hard pulse with the same duration of 8000 μs, the latter being about 0.73 μT, yielding a maximum BIR-4 amplitude of 13.05 μT. This choice was based on simulations programmed in MATLAB (The MathWorks, Inc., Natick, MA, USA), solving numerically the Bloch Equations via a Runge-Kutta procedure.[8] In detail, the simulations showed that, for the given choice of parameters, a single BIR-4 pulse yields effective excitation angles of 89.8° for $B_1 = 1$, 88.6° for $B_1 = 0.7$, and 89.7° for $B_1 = 1.3$, thus being relatively immune to the range of B_1 deviations that have been reported as typical for a 3T MRI system.[9] Due to the relatively long duration of the BIR-4 pulse as used in this study, there is a certain susceptibility to distortions of the static magnetic field B_0. In the bulk part of the brain, B_0 deviations of up to 0.5 ppm can be expected,[10] corresponding to Larmor frequency offsets of up to 64 Hz on a 3T system. Simulations showed that in this case the effective excitation angle for the described pulse is still 88.2°. In areas of strong B_0 distortions such as the orbitofrontal cortex, due to the vicinity of the nasal sinus, B_0 offsets amount to about 1 ppm,[10] yielding an effective excitation angle of 85.7°.

To further improve the saturation efficiency, in particular for high B_1 deviations and strong B_0 offsets, two subsequent BIR-4 pulses were used, including three interleaved spoiler gradients with durations of 40 ms. To avoid echo formation induced by the BIR-4 pulses, an exponential increase of spoiler gradient amplitudes was chosen, amounting to 1 mT/m (before the first BIR-4 pulse), 2 mT/m (between both BIR-4 pulses), and 4 mT/m (after the second BIR-4 pulse). In this way, the sum of two arbitrary spoiler gradient moments is always different from the third spoiler gradient moment, thus reducing the risk of echo formation. The relatively long duration of 40 ms was chosen deliberately to maintain small gradient amplitudes, thus minimizing concomitant acoustic noise. In the presence of long T_2, for example, in CSF, there may be a certain risk that the excitation pulses of an EPI acquisition act as refocusing pulses, yielding spin echo formation. To reduce this effect, opposite gradient polarities were chosen for the spoiler gradients in silent periods prior to and following each EPI acquisition.

2.2 | Simulation

To highlight the importance of a full saturation in the SEPIMS sequence, signal amplitudes in even and odd volumes were simulated, assuming for spin saturation a standard hard pulse (rather than an adiabatic pulse) that is affected by B_1 inhomogeneities in the same way as the excitation pulse. Simulations were performed for three different conditions: (1) no saturation (flip angle of the saturation pulse $FA_{SAT} = 0°$) but full excitation (flip angle of the EPI excitation $FA_{EX} = 90°$) (ie, standard EPI rather than SEPIMS); (2) incomplete saturation and excitation, assuming 5% reduction in B_1, so $FA_{SAT} = FA_{EX} = 0.95*90°$; and (3) full saturation and excitation ($FA_{SAT} = FA_{EX} = 90°$). Other parameters used in the simulation were: repetition time (TR) = 2 s, T_1 = 850 ms/1400 ms/4500 ms for WM/GM/CSF,[11,12] two different delay combinations $\tau_1/\tau_2/\tau_{sat}$ = 1 s/20 s/0.5 s and 6 s/20 s/3 s, 100 volumes. In detail, an initially fully relaxed spin system was assumed, modeling subsequently the longitudinal magnetization during the following process: T_1-relaxation during $\tau_1 - \tau_{sat}$, complete or partial saturation with FA_{SAT}, T_1-relaxation during τ_{sat}, excitation with FA_{EX}, T_1-relaxation during TR, followed by the same procedure, using τ_2 rather than τ_1. This was repeated recursively for 100 volumes, assuming the T_1 values of WM, GM, or CSF. For the last pair of odd/even volumes where steady-state conditions can be assumed, signal intensities were derived for each tissue type by multiplying the respective longitudinal magnetization directly before excitation with $\sin(FA_{EX})$. Simulations were performed using custom built scripts written in MATLAB (The MathWorks, Inc., Natick, MA, USA).

2.3 | Experiments

The purpose of the phantom and in-vivo experiments described below was to compare the signal stabilities of SEPIMS and CS-EPI sequences. In particular, the goal was to test the signal stability in SEPIMS data for three saturation modules (no saturation, SSP, DSP) and with different gradient spoilers after each EPI readout to assess the influence of eddy currents.

All data were acquired on a 3T whole-body MRI scanner (MAGNETOM Prisma, Siemens, Erlangen, Germany), using a body-TX coil and a 64-channel phased-array head-RX coil. The in-vivo scans were approved by the local ethics committee of the University hospital. Written informed consent was obtained from all participants before scanning.

The parameters of the EPI module were identical for all SEPIMS and CS-EPI experiments described below: TR/TE = 2000 ms/30 ms, FOV = 192 × 192 mm^2, matrix size = 64 × 64, spatial resolution = 3 × 3 mm^2, 30 axial slices (thickness = 2 mm, gap = 1 mm), full Fourier encoding, no parallel imaging techniques, echo-spacing = 0.5 ms, bandwidth = 2298 Hz/pixel. The listed TR refers to the acquisition time for a single EPI volume and does not comprise the inter-volume delay. The basic timings for CS-EPI and SEPIMS acquisitions are shown in Figure 2. In CS-EPI, a constant inter-volume delay of 20 s is inserted between EPI volumes. In SEPIMS, two different delay combinations (τ_1/τ_2 = 1 s/20 s for in-vitro experiments and 6 s/20 s for both in-vitro and in-vivo experiments) are inserted before odd/even volumes, respectively. It should be noted that scanner noise occurs only during EPI acquisitions.

For all in vitro SEPIMS experiments, two types of spoiler gradients following each EPI readout were tested:

1. Strong spoiler gradients after each EPI readout to investigate potential effects of eddy currents: spoiler gradients were switched simultaneously along readout, phase and slice encoding directions, amplitude: identical to readout gradient (>20 mT/m), ramp time: 1 ms, flat top duration: 1 ms.
2. Weak spoiler gradients with increased ramp times after each EPI readout to minimize eddy currents: spoiler gradients were switched only in the readout direction, amplitude: 15 mT/m, ramp time: 2 ms, flat top duration: 1 ms.

2.4 | In-vitro experiment: Water phantom

To assess the SEPIMS signal stability for long T_1 values, a bottle was filled with tap water which has a T_1 of about 3 s at room temperature.[13] It should be noted that the exact T_1 value was not measured and depends on parameters such as the specific ion concentrations in the case of non-distilled water and the exact temperature. To avoid convection, the bottle resided in the magnet bore for a duration of 30 min before starting the scans. The following scans were performed, all with an identical EPI readout, as described above:

1. CS-EPI, constant delay of 20 s between EPI modules, 50 volumes, total duration 18:00 min.
2. SEPIMS, $\tau_1/\tau_2/\tau_{sat}$ = 1 s/20 s/0.5 s, 50 volumes, total duration 10:25 min. Three versions were acquired with different saturation modules:
3. No saturation (NS).
4. Single adiabatic saturation pulses as shown in Figure 1B.
5. Dual adiabatic saturation pulses as proposed and as shown in Figure 1C.
6. SEPIMS, $\tau_1/\tau_2/\tau_{sat}$ = 6 s/20 s/3 s, 50 volumes, total duration 12:30 min. Three versions were acquired with different saturation modules, as described in 2a-2c.

To assess the effect of eddy currents, all SEPIMS experiments were performed twice, either using strong or weak spoiler gradients after each EPI readout (see above).

2.5 | In-vitro experiment: Gel phantom

The phantom consisted of a spherical glass container with a diameter of 166 mm, which was filled homogeneously with agarose gel (1.75% w/v agarose dissolved in 0.9% NaCl solution and doped with gadolinium diethylenetriamine pentaacetic acid at a concentration of 0.11 mmol/L), as described in the literature.[14] It has been shown that the T_1 value of this phantom at 3T is approximately 900 ms,[15] roughly corresponding to the T_1 of WM at the same field strength. Identical experiments as for the water phantom were performed.

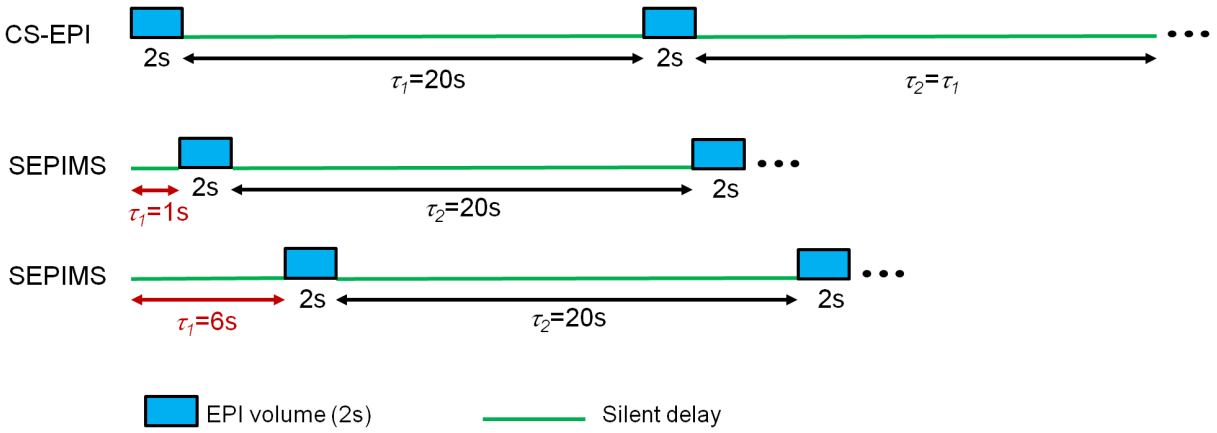

FIGURE 2 Timing for the different CS-EPI and SEPIMS acquisitions. In CS-EPI, a constant silent inter-volume delay of 20 s is inserted between EPI volumes. In SEPIMS, two different delay combinations (τ_1/τ_2 = 1 s/20 s and 6 s/20 s) are inserted before odd/even volumes, respectively. Scanner noise occurs during EPI acquisitions, only

2.6 | In-vivo experiment

Two healthy volunteers (one female, one male; age, 24-24.3 years) were scanned. The EPI module was identical to the in-vitro experiments. The following scans were performed for each subject:

1. CS-EPI, constant delay of 20 s between EPI modules, 40 volumes, total duration 14:20 min.
2. SEPIMS, $\tau_1/\tau_2/\tau_{sat}$ = 6 s/20 s/3 s, 40 volumes, total duration 10:00 min. Three versions were acquired with different saturation modules, as described above. Weak gradient spoilers were used to reduce eddy currents.

Furthermore, for each single run an additional reference volume was acquired with reversed phase gradient polarities to allow for image distortion correction using the TOPUP concept.[16,17]

2.7 | Image analysis

For all scans, the first two volumes were discarded, restricting analysis to the volumes for which steady-state conditions can be assumed.

All phantom data were analyzed according to the following two procedures which were applied to each single CS-EPI and SEPIMS run:

1. ROI based analysis: the ROI covered the whole FOV, that is, for each single volume of the respective run, signal intensities were added up across all pixels inside and outside the phantom, yielding the summative signal S(v) where v is the volume number. Please note that a restriction of the analysis to pixels inside the phantom via masking was deliberately avoided to maintain sensitivity to potential edge effects. The normalized time course $S(v)/S_{AV}$ was then displayed in a plot where S_{AV} is the average across all S(v).
2. fMRI analysis: for each run, a functional analysis was performed, testing for systematic deviations between even and odd volumes. This analysis was performed with BrainVoyager QX version 2.1.[18]

The in-vivo data were again analysed in two different ways:

1. ROI based analysis: Preprocessing was performed using the FMRIB Software Library (FSL, version 6.0.1).[17] All datasets were initially corrected for motion and registered to the first volume in the series with FMRIB's linear coregistration tool FLIRT.[19] Data were then corrected for geometrical distortions via the method implemented in TOPUP.[16,17] Subsequently, data were segmented, using the software tool FAST.[20] From the resulting tissue probability maps, ROIs comprising WM, GM, and CSF compartments were derived, using a lower probability threshold of 0.99. For each ROI, normalized signal fluctuations across all volumes were derived as described for the phantom experiment.
2. fMRI analysis: Preprocessing was performed using BrainVoyager QX, version 2.1.[18] Each dataset was corrected for inter-volume motion and also for different slice timing. No spatial filtering was applied. The stimulation protocol file was prepared by assuming for each odd volume the "ON" mode and for each even volume the "OFF" mode. This protocol file was used for calculating the linear correlation map. Threshold values [0.6 0.8] for in-vivo datasets were used, applying a false discovery rate (FDR) corrected threshold of $q < 0.05$[21] to avoid false positives.

3 | RESULTS

3.1 | Results of simulation

In the absence of saturation pulses, that is, for a standard EPI with different inter-volume delays, relative WM signal differences between even and odd volumes were 3% for the delay combination 1 s/20 s, and 0.01% for 6 s/20 s. In GM, the relative differences were 13.3% and 0.3%, respectively. In contrast, the relative signal differences for CSF were 104% and 19.4%, respectively. These differences will yield a marked bias, in particular for CSF compartments, but also for GM areas with a certain CSF content due to partial volume effects, such as in cortical GM. For SEPIMS with full saturation, signal levels were identical for even and odd volumes in all compartments.

For SEPIMS with incomplete saturation due to a 5% reduction in B_1 and a delay combination of 1 s/20 s, signal differences between even and odd volumes were 0.5%, 2.6%, and 28.87% for WM, GM, and CSF, respectively. Please note in particular the strong signal difference for CSF that is induced by a relatively minor B_1 reduction of only 5%. For SEPIMS with incomplete saturation and a delay combination of 6 s/20 s, relative signal differences between even and odd volumes were negligible for WM and GM (less than 0.1%), but still amounted to 2.4% for CSF. This discrepancy is not negligible as it may exceed the relatively small signal changes induced by the hemodynamic response. In summary, the results of the simulation stress the importance of a high saturation efficiency in SEPIMS that cannot be achieved with a standard hard pulse, rather requiring adiabatic saturation pulses.

3.2 | Results of experiments

3.2.1 | In-vitro experiment: Water phantom

Figure 3 shows the results of the ROI analysis, both for the delay combinations 1 s/20 s (Figure 3A) and 6 s/20 s (Figure 3B). The displayed time courses refer to the reference CS-EPI (Figure 3, black), SEPIMS without saturation (Figure 3, red), SEPIMS with SSP (Figure 3, blue), and SEPIMS with DSP (Figure 3, green). The first column shows the signal time course for CS-EPI and SEPIMS with weak spoiler gradients after the EPI readout. There is a marked signal bias between even and odd volumes if SEPIMS without saturation is used (Figure 3, red), in particular for the combination 1 s/20 s (Figure 3A). This is due to the fact that a delay of 1 s is too short to allow for full spin relaxation inside the phantom. Still, even for the combination 6 s/20 s (Figure 3B), a marked discrepancy between even and odd volumes is visible for SEPIMS without saturation (Figure 3, red). The second column shows the same results, omitting the curve for SEPIMS without saturation, thus allowing to display data with different scaling. For the combination 1 s/20 s (Figure 3, top), SEPIMS with SSP (Figure 3, blue) still shows a certain discrepancy between even and odd volumes which is less pronounced for the combination 6 s/20 s (bottom). In contrast, SEPIMS with DSP (Figure 3, green) provides similar signal stability as the CS-EPI reference (Figure 3, black). The drift in the data most probably arises from a B_0 field drift which has been reported for EPI data in previous studies[22,23]: mechanical vibrations of the gradient coil due to the strong and rapidly oscillating readout gradient yield frictions between vibrating parts and thus a concomitant temperature increase. Heating of ferromagnetic shim elements that are attached to the gradient coil leads to magnetization losses, thus changing the homogeneity and amplitude of the static magnetic field B_0. In fact, linear B_0 changes and successive broadening of the resonance lines have been reported to occur during EPI measurements,[22] yielding detuning of the RF coils and successive T_2^* shortening

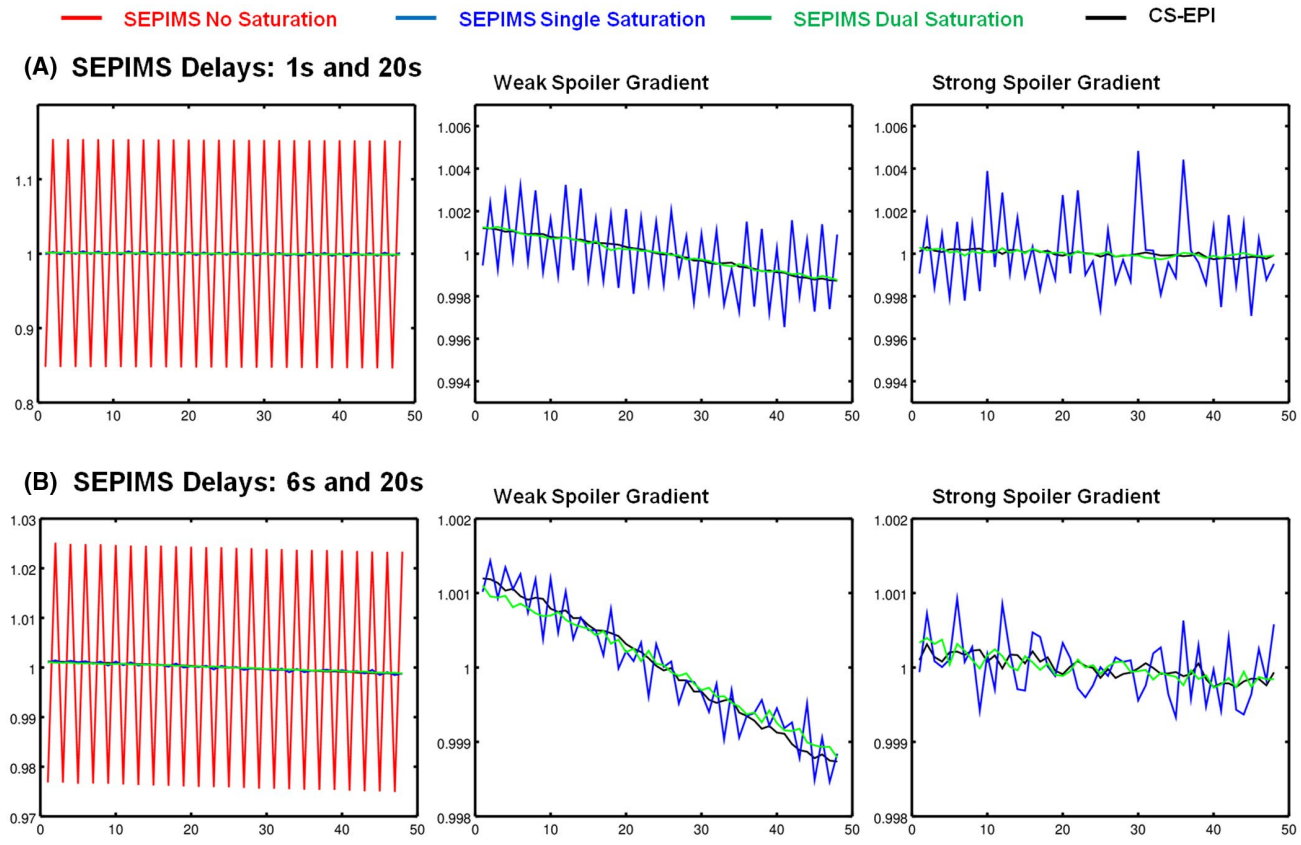

FIGURE 3 Results for the water phantom: ROI analysis for two delay combinations 1 s/20 s (A) and 6 s/20 s (B). Signal time courses refer to the reference CS-EPI (black), SEPIMS without saturation (red), SEPIMS with single saturation (blue), and SEPIMS with dual saturation (green). The first two columns show the results of CS-EPI and SEPIMS with weak spoiler gradients. The second column shows the same results as the first column, omitting the data for SEPIMS without saturation, allowing to zoom in on values close to 1.0. There is a marked signal bias between odd and even volumes for SEPIMS without saturation (red). For the delay combination 1 s/20 s (A), SEPIMS with single saturation (blue) still shows a minor discrepancy between odd and even volumes. In contrast, SEPIMS with dual saturation (green) provides similar signal stability as the CS-EPI reference (black). The third column shows the respective results for SEPIMS with strong spoiler gradients

induced by the loss of field homogeneity. In particular the latter effect is most likely the origin of the observed drift, given the marked T_2^* weighting of EPI data.

The third column of Figure 3 shows the respective results for SEPIMS with strong spoiler gradients after the EPI readout, yielding similar findings. However, the signal stability of SEPIMS with SSP (Figure 3, blue) is slightly worse than for the data acquired with weak spoiler gradients (Figure 3, second column).

Figure 4 shows the results of the fMRI analysis for the two different delay combinations 1 s/20 s (Figure 4A) and 6 s/20 s (Figure 4B). The standard CS-EPI (Figure 4, first column) yields no false activations since there is no signal difference between even and odd volumes. SEPIMS without saturation (NS) (Figure 4, second column) yields strong pseudo activation across the whole phantom, due to signal discrepancies between odd and even volumes. SEPIMS with SSP (Figure 4, third column) shows residual pseudo activation due to insufficient spin saturation. This is more pronounced if one of the inter-volume delays is short relative to the phantom T_1 value (Figure 4A). The proposed SEPIMS with DSP and weak spoiler gradients after the EPI readout (Figure 4, fourth column, red frame) is free from pseudo activations for both delay combinations. In contrast, SEPIMS with DSP and strong spoiler gradients (Figure 4, fifth column) suffers from eddy-current distortions for the delay combination 1 s/20 s, yielding edge artifacts as indicated by red arrows (Figure 4A, see also zoomed version at the bottom). For the long inter-volume delay combination 6 s/20 s, eddy currents have sufficient time to decay, mitigating such artifacts (Figure 4B).

3.2.2 | In-vitro experiment: Gel phantom

Figure 5 shows the results of the ROI analysis. The arrangement is identical to Figure 3. The main findings are similar to those of the water phantom but in general less marked, due to the shorter T_1 value of the gel phantom. Again, SEPIMS with DSP (Figure 5, green) provides similar signal stability as the CS-EPI reference (Figure 5, black) for all inter-volume delay combinations and spoiler gradient strengths. In contrast to the water phantom, SEPIMS with SSP (Figure 5, blue) shows no signal discrepancies for the inter-volume delay combination 6 s/20 s (Figure 5B, second and third column).

Figure 6 shows the results of the fMRI analysis for the delay combination 1 s/20 s, only, comparing data acquired

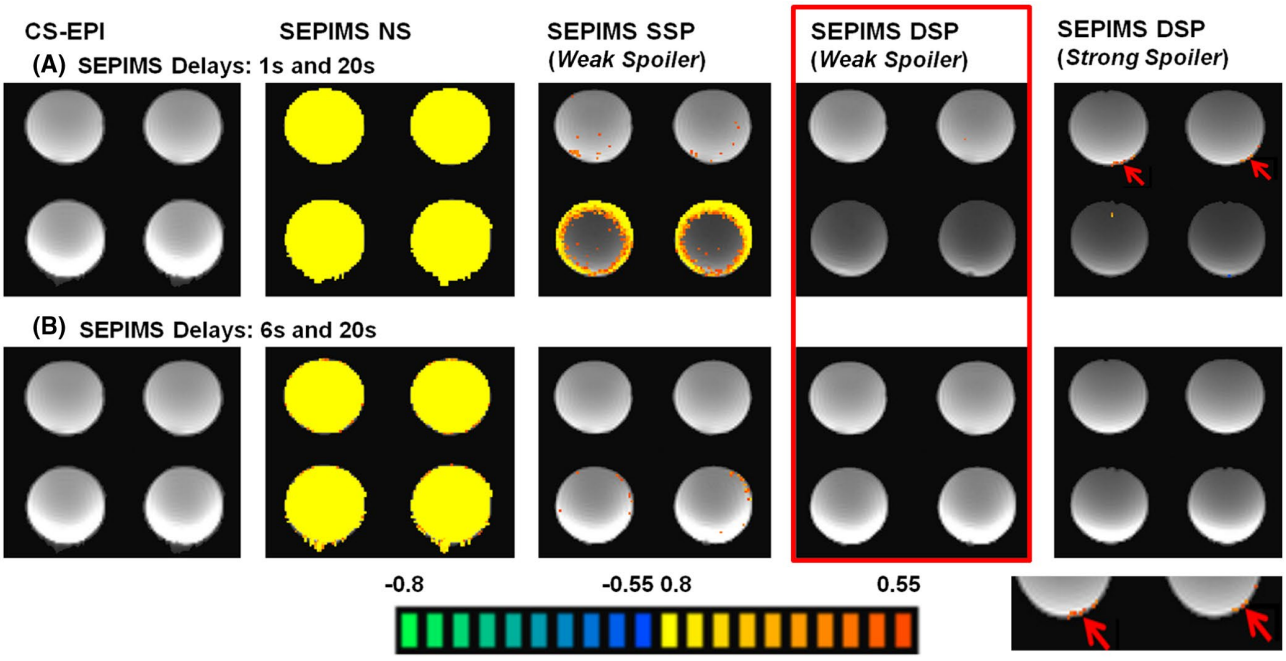

FIGURE 4 Results for the water phantom: fMRI analysis (activation maps) for the delay combinations 1 s/20 s (A) and 6 s/20 s (B), using weak or strong spoiler gradients after the EPI readout. First column: Standard CS-EPI yields no false activations. Second column: SEPIMS without saturation (NS) yields strong pseudo activation due to signal discrepancies between odd and even volumes. Third column: SEPIMS with single saturation pulse (SSP) generates residual activation due to insufficient saturation. A, This is more pronounced for the inter-volume delay combination 1 s/20 s since the first delay is short. Fourth column (red frame): The proposed SEPIMS with dual saturation pulse (DSP) shows no false activations for both delay combinations. Fifth column: SEPIMS with DSP and strong spoiler gradients suffers for the delay combination 1 s/20 s from eddy-current distortions yielding edge artifacts as indicated by red arrows (A, zoomed version at bottom). B, The use of the inter-volume delay combination 6 s/20 s allows for a decay of eddy currents, thus mitigating such artifacts. The color scale indicates the t-score (FDR corrected threshold: $q < 0.05$)

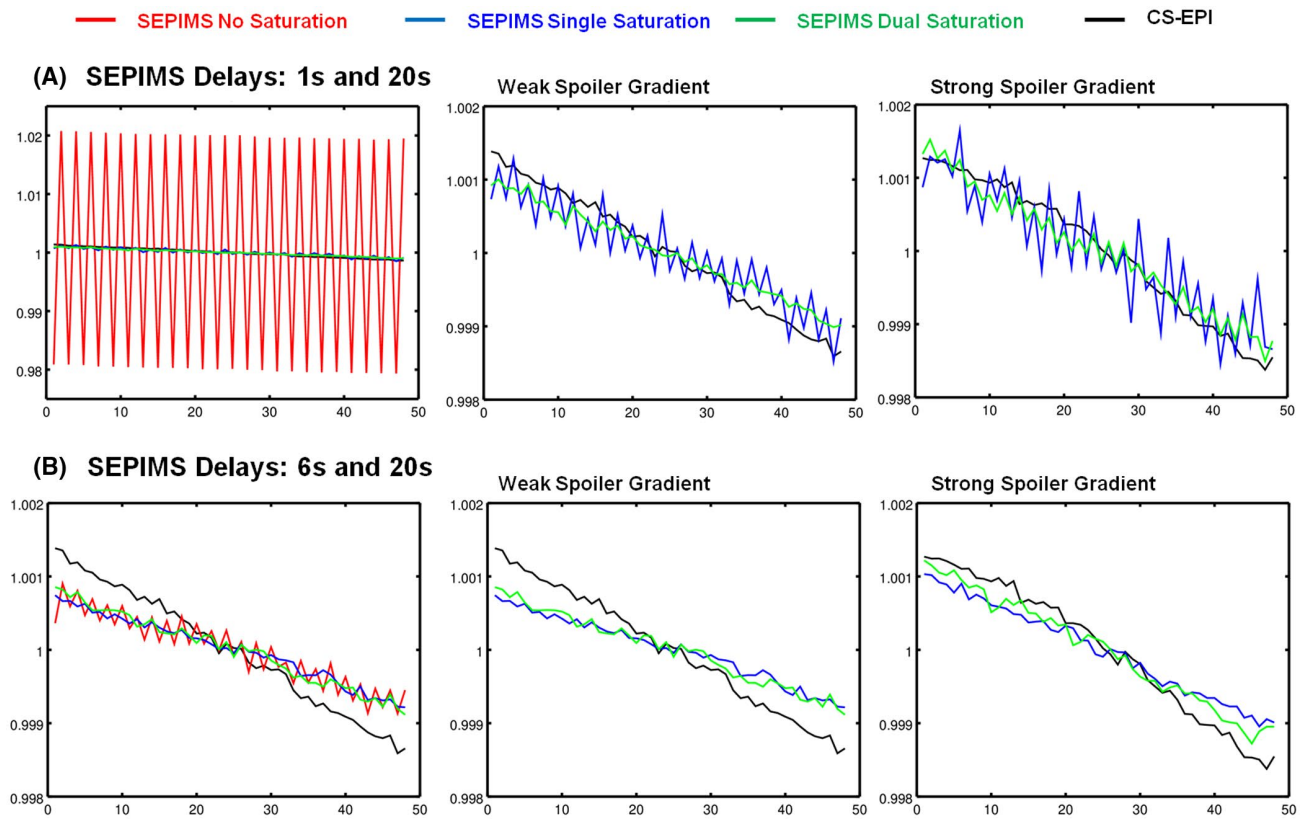

FIGURE 5 Results for the gel phantom: ROI analysis for two delay combinations 1 s/20 s (A) and 6 s/20 s (B). The arrangement is identical to Figure 3. Main findings are similar to those of the water phantom, but less marked due to the shorter T_1 value of the gel phantom. Again, SEPIMS with dual saturation (green) provides similar signal stability as the CS-EPI reference (black). SEPIMS with single saturation (blue) shows residual discrepancies between even and odd volumes for the delay combination 1 s/20 s, only

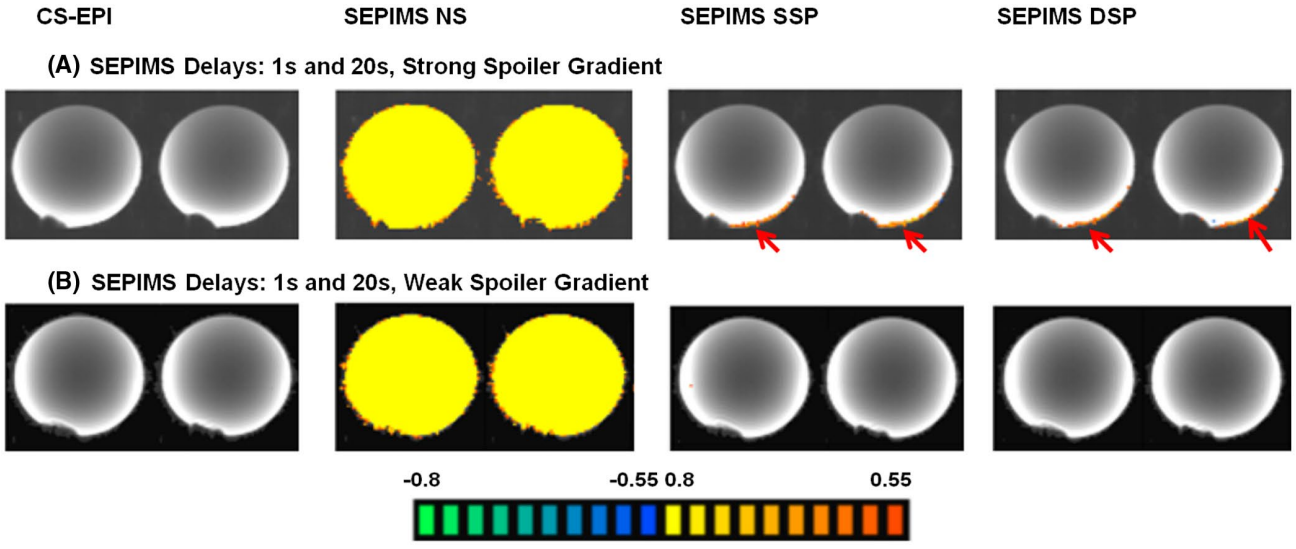

FIGURE 6 Results for the gel phantom: fMRI analysis (activation maps) for the delay combination 1 s/20 s, using strong (A) and weak (B) spoiler gradients. The standard CS-EPI (first column) yields no false activations. SEPIMS without saturation (second column) yields strong pseudo activation. SEPIMS with single (third column) or dual (fourth column) saturation shows in the case of strong spoiler gradients (A) false activation close to the phantom edges (red arrows), most likely due to eddy-current related distortions, while for weak spoiler gradients (B), no false activations are detected. The color scale indicates the t-score (FDR corrected threshold: $q < 0.05$)

with strong (Figure 6A) and weak (Figure 6B) spoiler gradients after the EPI readout. Standard CS-EPI (first column) yields no false activation. SEPIMS without saturation (Figure 6, second column) yields strong pseudo activation due to signal discrepancies between odd and even volumes. SEPIMS with SSP (Figure 6A, third column) or DSP (Figure 6A, fourth column) yields slight edge artifacts (pseudo activation) due to eddy-current distortions arising from the strong spoiler gradients. When using weak spoiler gradients, SEPIMS with SSP (Figure 6B, third column) or with DSP (Figure 6B, fourth column) is free from edge artifacts.

3.2.3 | In-vivo experiment

Figure 7 shows normalized signal time courses for subject 1 in CSF (Figure 7, blue), GM (Figure 7, red) and WM (Figure 7, green). Results refer to CS-EPI (Figure 7, top left), SEPIMS without saturation (Figure 7, top right), SEPIMS with SSP (Figure 7, bottom left), and SEPIMS with DSP (Figure 7, bottom right). If SEPIMS without saturation is used, there is a marked discrepancy between even and odd volumes, in particular for CSF (Figure 7, blue), due to the long T_1, but also for GM (Figure 7, red) and, to a certain degree, for WM (Figure 7, green). In contrast, SEPIMS with SSP and with DSP provides comparable signal stability. Data from subject 2 (not shown) yielded identical findings. As for the phantom experiment, there appears to be an intensity drift in the CS-EPI data, which affects only the results for CSF, but not for WM and GM. The reason is probably the longer T_2^* value of CSF that is a consequence of the higher B_0 field homogeneity in CSF compartments, as they do not contain any tissue microstructure. Thus, the T_2^* value of CSF can be assumed to be more affected by field inhomogeneities induced by gradient coil and shim element heating, as explained above.

Figure 8 shows three slices of the fMRI results for subject 1. CS-EPI (Figure 8, top left) yields no false activation. SEPIMS without saturation pulses (Figure 8, top right) yields strong pseudo activation due to signal discrepancies between odd and even volumes, in particular for compartments with long T_1 values such as CSF or GM close to CSF. SEPIMS with SSP (Figure 8, bottom left) yields residual activation, in

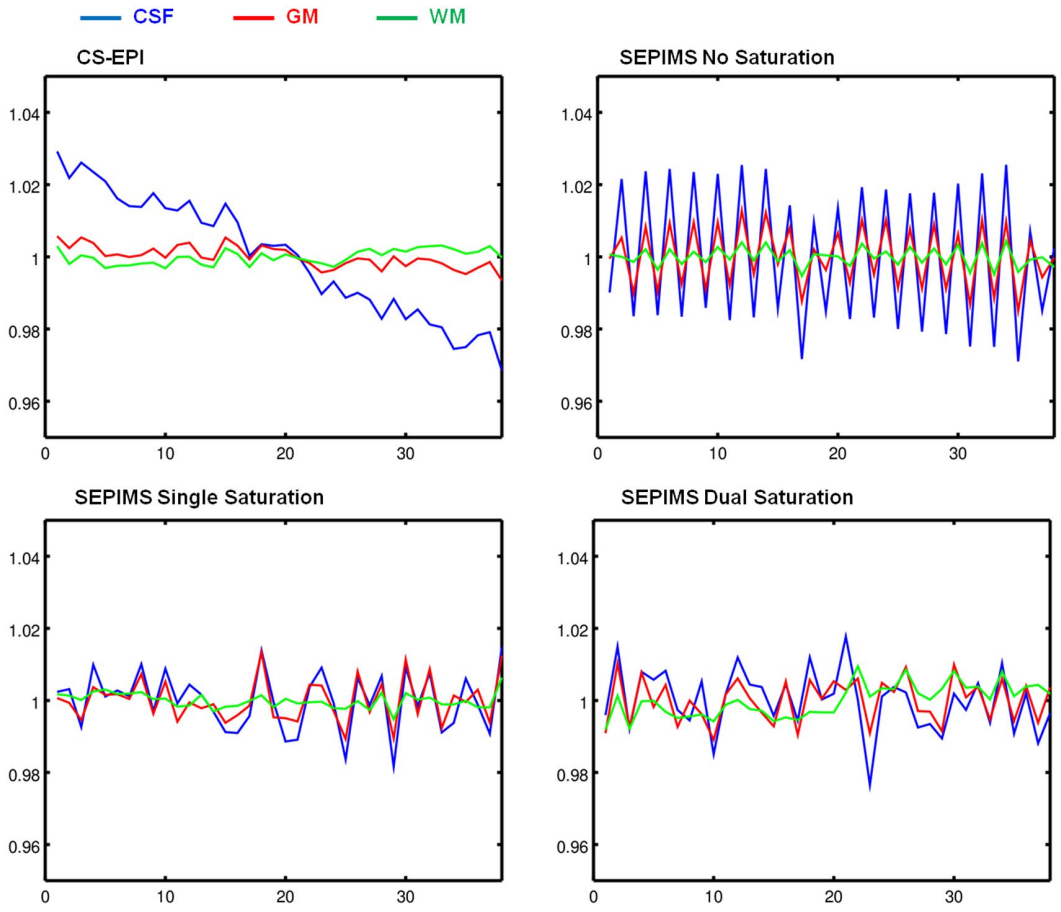

FIGURE 7 Normalized signal time courses for subject 1 in CSF (blue), GM (red), and WM (green). Results are shown for CS-EPI (top left), SEPIMS without saturation (top right), SEPIMS with single saturation (bottom left), and SEPIMS with dual saturation (bottom right). The discrepancy between even and odd volumes for SEPIMS without saturation decreases with the T1 value of the respective tissue type: CSF (blue), GM (red), and WM (green). In contrast, SEPIMS with single and with dual saturation provides comparable signal stability

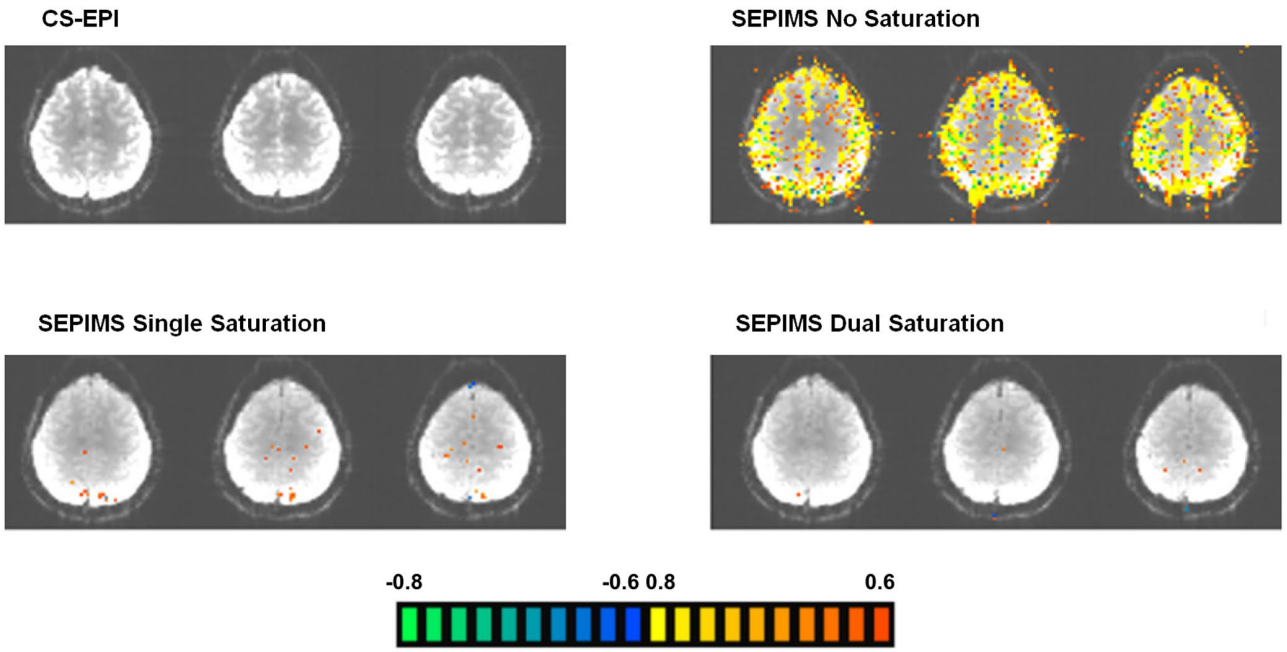

FIGURE 8 fMRI results for subject 1. CS-EPI (top left) yields no false activation. SEPIMS without saturation pulses (top right) yields strong pseudo activation, in particular inside or close to CSF. SEPIMS with single saturation (bottom left) yields residual activation, in particular in the top slices which were acquired first. The proposed SEPIMS with dual saturation (bottom right) shows no false activation. The color scale indicates the t-score (FDR corrected threshold: $q < 0.05$)

particular in the top slices, that is, in the slices acquired first, yielding the shortest delay between saturation and acquisition. In contrast, SEPIMS with DSP (Figure 8, bottom right) is free from pseudo activations.

4 | DISCUSSION

In this study, a novel fMRI sequence dubbed SEPIMS (pre-Saturated EPI using Multiple delays in Steady-state) is proposed that improves the flexibility in auditory fMRI experiments by allowing for silent inter-volume delays of variable duration while maintaining the steady state. The rationale is that the use of both short and long inter-volume delays allows for the acquisition of more EPI volumes during the same scan time than the commonly used CS-EPI sequence with constant inter-volume delays, thus improving the statistical power. SEPIMS is based on applying spin saturation at a fixed delay τ_{sat} before each EPI volume. In this way, the signal intensity depends only on the delay τ_{sat}, but not on the length of any delay previous to the saturation module. Thus, SEPIMS allows for the introduction of arbitrary pre-saturation delays without generating a delay dependent signal level. SEPIMS was tested for signal stability and artifacts, both in vitro and in vivo. In particular, it was investigated if secondary effects such as insufficient saturation efficiency or eddy currents may yield a residual dependence of the signal on delay durations, resulting in pseudo activation upon fMRI analysis of the data.

Both ROI based and fMRI results for a water phantom ($T_1 \approx 3$ s) and a gel phantom ($T_1 \approx 1$ s) show that SEPIMS with DSP yields a high signal stability, comparable to CS-EPI. In contrast, SEPIMS with SSP yields a residual signal dependence on the delay duration, in particular for long T_1 values and for marked differences between the delays chosen. This finding was confirmed by the in vivo experiment where SEPIMS with SSP yielded minor pseudo activation in the slices acquired first, in contrast to SEPIMS with DSP. Furthermore, the in-vitro data showed that great care has to be taken to reduce eddy currents that may originate from spoiler gradients applied after the EPI readout. This measure is essential since eddy currents would cause distortions in the subsequent EPI images for short inter-volume delays, thus yielding a delay dependent effect which would result in pseudo activations upon fMRI analysis.

The SEPIMS sequence as proposed here has certain limitations. First, the simulation and the experimental data show that the saturation efficiency has to be extremely high to reduce residual signal variations correlating with delay durations below a level which is typical for the hemodynamic response induced by auditory activation. For B_1 variations that are common on a 3T system (variation of up to $\pm 30\%$), the pulse design described in this work can be used. However, for stronger B_1 variations that may occur on high field systems, an improved design may be required.

Second, the spoiler gradients following each EPI readout have to be designed in a way that minimizes eddy currents.

As this effect depends on the scanner hardware, a general advice on the optimum design cannot be given here, so careful in-vitro testing is required.

Third, the insertion of very short inter-volume delays is problematic, as this would require a reduction of the saturation delay τ_{sat} (see Figure 1), which would markedly reduce the acquired signal if τ_{sat} is considerably shorter than the T_1 value of brain tissue.

A further problem may arise if a head coil is used for RF transmission. In this case, the adiabatic saturation pulses would only influence spins in the head and neck area, but not spins entering this area after saturation, such as spins from inflowing blood. In the present study, adverse effects were avoided using a body transmit coil. However, unsaturated inflowing blood spins may have an impact if a head transmit coil is used, such as on dedicated head scanners or high field scanners for reducing the specific absorption rate. A potential solution would be to use spin tagging, saturating spins inside a slab through the neck at regular intervals, thus reducing signal from blood.[24]

In this study, continuous EPI without inter-volume delays was not included for comparison as scanner noise during application of stimuli consisting of artificial sounds with simple structures affects the auditory processing of this stimulus type. The reason is that artificial sounds can be easily masked by scanner noise generated by fast gradient switching. Thus, CS-EPI was used as a standard method for comparison. The proposed SEPIMS sequence as well as CS-EPI acquires only a single volume after each silent period. A previous study[25] has shown that the ISSS scheme allows for collection of several volumes after each dummy scan period. However, this period contains slice selective excitation pulses to maintain the steady state, yielding residual acoustic noise from gradient switching. Still, due to the increased number of sampling points, the ISSS scheme may yield a significant gain in fMRI sensitivity over standard sparse schemes, being thus ideally suited for the presentation of music and speech stimuli which are robust to noise. Such stimuli are not easily masked by scanner noise and do not have complicated acoustic structures. In contrast, sparse sampling schemes may be better suited for stimuli with complicated acoustic structures, as they provide completely silent periods. Furthermore, the implementation of simultaneous multi-slice acquisition techniques may be advantageous in SEPIMS as they reduce the EPI acquisition time.[26]

The SEPIMS scheme allows for variable inter-volume delays, but requires a constant saturation delay τ_{sat} between saturation and EPI acquisition. As can be seen in Figure 1, τ_{sat} is the lower limit of the inter-volume delays. In one of the phantom experiments, the shorter delay was 1 s. However, under in vivo conditions, the concomitantly short τ_{sat} would result in low signal-to-noise ratio (SNR) values, so $\tau_{sat} \geq 3$ s is recommended which represents the lower limit for the shorter inter-volume delay.

fMRI experiments based on a block design allow to compare hemodynamic responses of two or more conditions. The option to use variable inter-volume delays facilitates the simultaneous assessment of both the peak BOLD response (which occurs about 6 s after a typical acoustic stimulus) and the baseline (which is attained after an approximately two to three times longer delay). Thus, in SEPIMS, values of 6 s and 12 s for the short and long inter-volume delay, respectively, are fully sufficient to capture both the early and the later part of the hemodynamic response. In contrast, CS-EPI rather uses the longer inter-volume delay. Thus, SEPIMS allows to acquire more volumes than CS-EPI during the same measurement time. As a consequence, the fMRI sensitivity of SEPIMS can be expected to be higher or at least similar to conventional sparse sampling, yielding an improved temporal SNR and a reduced FDR.

Still, it has to be stressed that SEPIMS requires a careful protocol optimization, as very short values of τ_{sat} reduce the SNR, whereas long values yield long inter-volume delays and thus less sampling points per time which reduces the fMRI sensitivity.

SEPIMS allows for a more flexible auditory stimulus design, thus offering the advantage of a wider range of experimental setups. As an example, after presentation of an auditory stimulus, EPI volumes can be collected with different delays, giving information on the timing of the hemodynamic response. A further advantage of SEPIMS would be the reduction of scan durations as the silent delay for auditory stimulus presentation can be adapted to the individual stimulus length instead of being restricted to a constant delay determined by the longest stimulus length.

A potential application of SEPIMS would be the investigation of the hemodynamic response elicited by scanner noise: by carefully choosing the intervals between EPI volumes, the preceding volume would trigger the hemodynamic response and the subsequent volume would capture the delayed hemodynamic response in the auditory cortex. A previous study[27] implemented for this purpose dummy volumes without RF transmission to capture the hemodynamic response curves in response to typical TRs of 1 s and 1.5 s. These dummy volumes served merely for the generation of imaging noise and were followed by EPI acquisition. An extra null condition was added to acquire the baseline. The advantage of the SEPIMS scheme would be that the first volume of each pair directly serves as the baseline for the following volumes with varying delays. This proximate acquisition of the baseline and the activation reduces the variance.

A further application of SEPIMS would be the measurement of the exact timing of a BOLD response to an acoustic stimulus. The constraint of CS-EPI is a constant inter-volume

delay for maintaining the longitudinal magnetization. Thus, the audio stimuli have to be segmented to fit into the inter-volume delays. However, since the neural response is neither regularly spaced nor segmented, one has to find a sophisticated time shifting scheme of the segmented stimuli to capture accurately the timing of the investigated BOLD response. This poses a problem to more naturalistic experimental settings with complex acoustic stimuli (such as narrations), where the events of interest (occurrence of varying voice pitch, feeling and emotion words) may occur at any moment within a continuous stream. The CS-EPI sequence with fixed intervals is less suited for experiments of this type. In contrast, the proposed SEPIMS scheme would allow to trigger the next volume acquisition by key events (such as the occurrence of words) at any time point.

5 | CONCLUSIONS

The proposed SEPIMS scheme allows for the acquisition of a series of EPI volumes, maintaining a high signal stability in the presence of variable inter-volume durations. This is achieved by using spin saturation at a fixed delay before each EPI volume to yield a well-defined longitudinal magnetization when acquisition starts, independent of previous spin history. Therefore, SEPIMS facilitates flexible and efficient stimulus design in auditory fMRI experiments. To avoid residual correlations between signal levels and inter-volume durations that would result in pseudo activation upon fMRI analysis, DSP are required for a sufficiently high saturation efficiency. Furthermore, spoiler gradient pulses after the EPI readout have to be optimized to avoid eddy-current-induced image distortions.

ACKNOWLEDGMENTS

Open access funding enabled and organized by Projekt DEAL.

ORCID

Manoj Shrestha https://orcid.org/0000-0002-0129-2397
Ulrike Nöth https://orcid.org/0000-0003-0699-4088
Ralf Deichmann https://orcid.org/0000-0002-4110-1225

REFERENCES

1. Mansfield P. Multi-planar image formation using NMR spin echoes. *J Phys C Solid State Phys*. 1977;10:L55.
2. Hall DA, Haggard MP, Akeroyd MA, et al. "Sparse" temporal sampling in auditory fMRI. *Hum Brain Mapp*. 1999;7:213-223.
3. Talavage TM, Edmister WB, Ledden PJ, Weisskoff RM. Quantitative assessment of auditory cortex responses induced by imager acoustic noise. *Hum Brain Mapp*. 1999;7:79-88.
4. Edmister WB, Talavage TM, Ledden PJ, Weisskoff RM. Improved auditory cortex imaging using clustered volume acquisitions. *Hum Brain Mapp*. 1999;7:89-97.
5. Schwarzbauer C, Davis MH, Rodd JM, Johnsrude I. Interleaved silent steady state (ISSS) imaging: A new sparse imaging method applied to auditory fMRI. *NeuroImage*. 2006;29:774-782.
6. Shrestha M, Hok P, Nöth U, Lienerth B, Deichmann R. Optimization of diffusion-weighted single-refocused spin-echo EPI by reducing eddy-current artifacts and shortening the echo time. *Magn Reson Mater Phys*. 2018;31:585-597.
7. Staewen RS, Johnson AJ, Ross BD, Parrish T, Merkle H, Garwood M. 3-D FLASH imaging using a single surface coil and a new adiabatic pulse, BIR-4. *Invest Radiol*. 1990;25:559-567.
8. Deichmann R. Fast high-resolution T1 mapping of the human brain. *Magn Reson Med*. 2005;54:20-27.
9. Volz S, Nöth U, Rotarska-Jagiela A, Deichmann R. A fast B1-mapping method for the correction and normalization of magnetization transfer ratio maps at 3 T. *NeuroImage*. 2010;49:3015-3026.
10. Li S, Dardzinski BJ, Collins CM, Yang QX, Smith MB. Three-dimensional mapping of the static magnetic field inside the human head. *Magn Reson Med*. 1996;36:705-714.
11. Volz S, Nöth U, Deichmann R. Correction of systematic errors in quantitative proton density mapping. *Magn Reson Med*. 2012;68:74-85.
12. Volz S, Nöth U, Jurcoane A, Ziemann U, Hattingen E, Deichmann R. Quantitative proton density mapping: Correcting the receiver sensitivity bias via pseudo proton densities. *NeuroImage*. 2012;63:540-552.
13. Nehrke K, Börnert P. DREAM—A novel approach for robust, ultrafast, multislice B1 mapping. *Magn Reson Med*. 2012;68:1517-1526.
14. Shrestha M, Nöth U, Deichmann R. Improved signal-to-noise ratio in EPI sequences with highly asymmetric spin echo and highly asymmetric STEAM preparations (HASE-EPI and HASTEAM-EPI). *Magn Reson Mater Phys*. 2019;32:549-558.
15. Gracien RM, Maiworm M, Brüche N, et al. How stable is quantitative MRI?—Assessment of intra-and inter-scanner-model reproducibility using identical acquisition sequences and data analysis programs. *NeuroImage*. 2020;207:116364.
16. Andersson JLR, Skare S, Ashburner J. How to correct susceptibility distortions in spin-echo echo-planar images: Application to diffusion tensor imaging. *NeuroImage*. 2003;20:870-888.
17. Smith SM, Jenkinson M, Woolrich MW, et al. Advances in functional and structural MR image analysis and implementation as FSL. *NeuroImage*. 2004;23:S208-S219.
18. Goebel R, Esposito F, Formisano E. Analysis of functional image analysis contest (FIAC) data with brainvoyager QX: From single-subject to cortically aligned group general linear model analysis and self-organizing group independent component analysis. *Hum Brain Mapp*. 2006;27:392-401.
19. Jenkinson M, Bannister P, Brady M, Smith S. Improved optimization for the robust and accurate linear registration and motion correction of brain images. *NeuroImage*. 2002;17:825-841.
20. Zhang Y, Brady M, Smith S. Segmentation of brain MR images through a hidden Markov random field model and the expectation-maximization algorithm. *IEEE T Med Imaging*. 2001;20:45-57.
21. Genovese CR, Lazar NA, Nichols T. Thresholding of statistical maps in functional neuroimaging using the false discovery rate. *NeuroImage*. 2002;15:870-878.
22. Foerster BU, Tomasi D, Caparelli EC. Magnetic field shift due to mechanical vibration in functional magnetic resonance imaging. *Magn Reson Med*. 2005;54:1261-1267.

23. Bollmann S, Kasper L, Vannesjo SJ, et al. Analysis and correction of field fluctuations in fMRI data using field monitoring. *NeuroImage*. 2017;154:92-105.
24. Deichmann R, Schwarzbauer C, Turner R. Optimisation of the 3D MDEFT sequence for anatomical brain imaging: Technical implications at 1.5 and 3 T. *NeuroImage*. 2004;21:757-767.
25. Mueller K, Mildner T, Fritz T, et al. Investigating brain response to music: A comparison of different fMRI acquisition schemes. *NeuroImage*. 2011;54:337-343.
26. De Martino F, Moerel M, Ugurbil K, Formisano E, Yacoub E. Less noise, more activation: Multiband acquisition schemes for auditory functional MRI. *Magn Reson Med*. 2015;74:462-467.
27. Hu S, Olulade O, Castillo JG, et al. Modeling hemodynamic responses in auditory cortex at 1.5 T using variable duration imaging acoustic noise. *NeuroImage*. 2010;49:3027-3038.

How to cite this article: Shrestha M, Lee HS, Nöth U, Deichmann R. A novel sequence to improve auditory functional MRI with variable silent delays. *Magn Reson Med*. 2021;85:883–896. https://doi.org/10.1002/mrm.28479